

Impact Response Analysis of Concrete Filled Steel Tubular Member for Collision of Tsunami Flotsam

Effendi, Mahmud Kori

Department of Architecture, Graduate School of Human-Environment Studies, Kyushu University :
Doctoral Program

Kawaguchi, Hiromitsu

Department of Architecture, Graduate School of Human-Environment Studies, Kyushu University :
Master's program

Minami, Kosho

Department of Architecture, Graduate School of Human-Environment Studies, Kyushu University :
Master's program

Kawano, Akihiko

Department of Architecture and Urban Design, Faculty of Human-Environment Studies, Kyushu
University : Professor

他

<https://doi.org/10.15017/1785469>

出版情報 : 都市・建築学研究. 28, pp.65-77, 2015-07-15. 九州大学大学院人間環境学研究院都市・建築
学部門

バージョン :

権利関係 :

Impact Response Analysis of Concrete Filled Steel Tubular Member for Collision of Tsunami Flotsam

津波漂流物の衝突を対象としたコンクリート充填鋼管部材の衝撃解析

Mahmud Kori EFFENDI^{*1}, Hiromitsu KAWAGUCHI^{*2}, Kosho MINAMI^{*2}, Akihiko KAWANO^{*3},
Toshihiko NINAKAWA^{*3}, Shintaro MATSUO^{*3}, Keigo TSUDA^{*4} and Masae KIDO^{*4}

マハムド コリ エフエンディ, 河口弘光, 南 幸翔, 河野昭彦,
蜷川利彦, 松尾真太郎, 津田恵吾, 城戸將江

The frame analysis program by using a stress-fiber model is employed to the impact response analysis. The members are modeled by beam-column elements with a cross section consisting of stress fibers. The collision model is developed to consider that Tsunami flotsam collides with the CFT specimens. The gap element is employed to model the contact and separation between Tsunami flotsam and CFT specimens. The precision of analytical models of the frame analysis is confirmed by the comparison with the impact test results. Being based on a parametric numerical study by the analysis, it is discussed the influence of axial load on an energy absorption capacity of a CFT member under impact loading. Furthermore, the ultimate capacity of a CFT member taking the account of the potential energy release by axial load, which is equal to the upper bound of input energy by impact load, is theoretically introduced. The concept of the ultimate impact capacities of CFT members is expected to construct the evaluation method of impact capacity of CFT structures.

Keywords: CFT Members, Impact Loading, Energy Absorption, Axial Load

キーワード:コンクリート充填鋼管部材、衝撃荷重、エネルギー吸収、軸荷重

1. Introduction

The frame analysis program by using a stress-fiber model¹⁾ is employed to the impact response analysis. The impact velocity is about 7m/sec and it is categorized as low velocity impact load, consequently, the collapse modes of the specimens are mainly overall flexural deformation even though the steel tubes slight deform locally at the contact surface with the head of a striker²⁾. Based on this phenomenon, the concrete filled steel tubes (CFT) specimens can be investigated by the frame analysis. The frame analysis saves the calculation time in comparison with the finite element method (FEM) analysis, so that it enables a large-scaled parametric study.

In this study, the collision model is developed to consider that Tsunami flotsam collides with the CFT specimens. The gap element is employed in order to deal with the contact and separation between the Tsunami flotsam and CFT specimens.

The studies related to impact response analysis have mostly adopted FEM analyses, because the main concern of

the previous studies is to clarify the local strength and the local failure at the collision area, which need the information of local deformation. Yousuf, et al³⁾ presented an experiment and a FEM analysis to study the behaviors of square CFT columns subjected to impact loads with or without pre-compressive axial load. Wang, et al⁴⁾ performed an experiment and a FEM analysis to study the performance of circular CFT members subjected to lateral impact loads. The effect of axial load is also considered. Han, et al⁵⁾ conducted a series of experiment on circular and square CFT members under transverse impact loads and a FEM model was proposed from the results of the experiment. In these studies, FEM analyses are adopted. On the other hand, impact response analyses based on frame analysis are scarcely found.

With respect to reinforced concrete (RC) members, the stress-fiber model was used by Fujikake, et al.⁶⁾, who investigated the behavior of RC beams subjected to the transverse impact loads by a drop hammer. The model of RC beam is composed of a couple of bar elements in longitudinal direction, and the cross-section of each element is subdivided into many layers each of which is a stress fiber. With respect to CFT members subjected to impact loads, no systematic studies by a frame analysis have been reported.

*1 空間システム専攻博士後期課程

*2 空間システム専攻修士課程

*3 都市・建築学部門, 九州大学

*4 国際環境工学部, 北九州市立大学

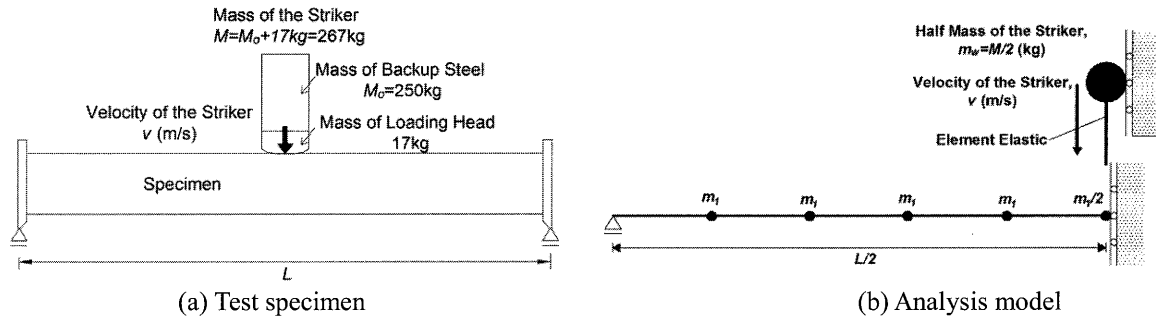
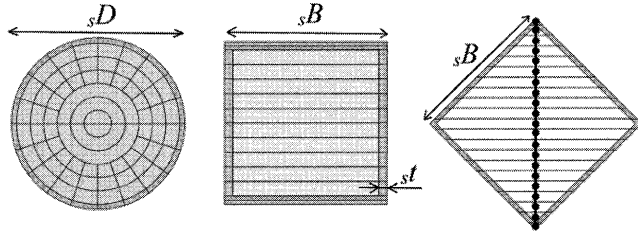


Fig. 1 Test specimen and analysis model



(a) Circular CFT (b) Square CFT (c) Diamond CFT
Fig. 2 Fiber discretization

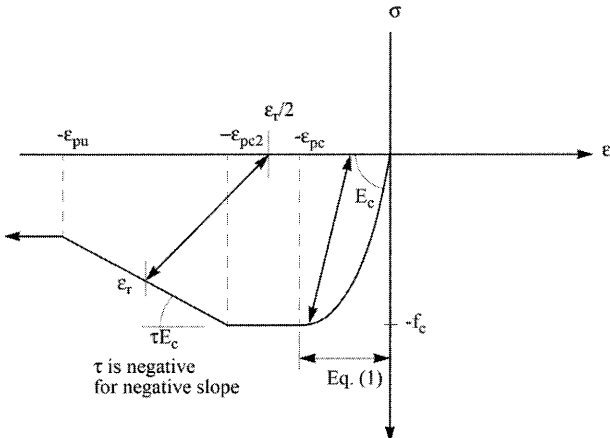


Fig. 3 Stress-strain relationship model for concrete fiber

2. Analysis Method

2.1 Outlines of Analysis

The analysis method is a plane frame analysis. The time incremental calculation is based on tangent stiffness relationships. The local coordinate system for each element moves with the rigid body displacements of the element, so that geometric nonlinearities are accurately handled for the full range of displacements. At each incremental step, the unbalanced forces at nodal points, which are obtained from the secant stiffness relationships, are resolved by the Newton-Raphson iterative procedure. The Newmark's method is applied to the time integration procedure, where the value of β is taken as 0.25 and the damping coefficients are specified by the Rayleigh damping.

The analytical model is a plane frame model, which is composed of a couple of beam-column elements in series to model the CFT member. Geometric nonlinearities are treated using an updated-Lagrangian formulation with a local

coordinate axis for each element, which moves with the element within the global axis system. The element stiffness is evaluated by the Gaussian numerical integrals. The stiffness of a cross section is numerically integrated by dividing the section into a number of layers referred to as stress fibers. The material nonlinearity is introduced by the stress-strain relationships of the stress fibers for steel and concrete portions. The increase of material strengths due to the strain rate effect is taken into account. The section response is obtained by the integration of stresses and strains of the fibers across the section. Appendix A contains the impact response analysis by earthquake response procedure.

2.2 Analysis Model of CFT Member

2.2.1 Analysis Model Composed of Beam-Column Elements with Stress Fibers

Fig. 1 (a) shows the CFT member, which is a simple beam and is subjected to transverse impact load by a striker. The analytical model is the half model in consideration of the symmetry, which is composed of five beam-column elements as shown in Fig. 1 (b). The lumped masses in the vertical and horizontal directions are set on the nodes except for the node at symmetry point which mass is a half of the mass at the other node. The striker with mass of m_w collides through an elastic element. The elastic element is in the form of gap element and elastic spring. Elastic spring has very small stiffness just to keep the integrity of the structural model and the analysis become stable when the gap element deformed. The gap element is used to model the contact and separation of the collision of the striker. The gap element has the equivalent stiffness as the steel cylinder with 200mm in diameter of the striker and the length is adjusted so as to match the impact response of the CFT specimen by the analysis with that by the experiment.

As shown in Fig. 2 (a), a steel tube portion of a circular CFT member is subdivided into one segment in the radius direction and twenty segments in the circumference direction. The concrete portion outside of the core is subdivided into three segments in the radius direction and twenty segments in

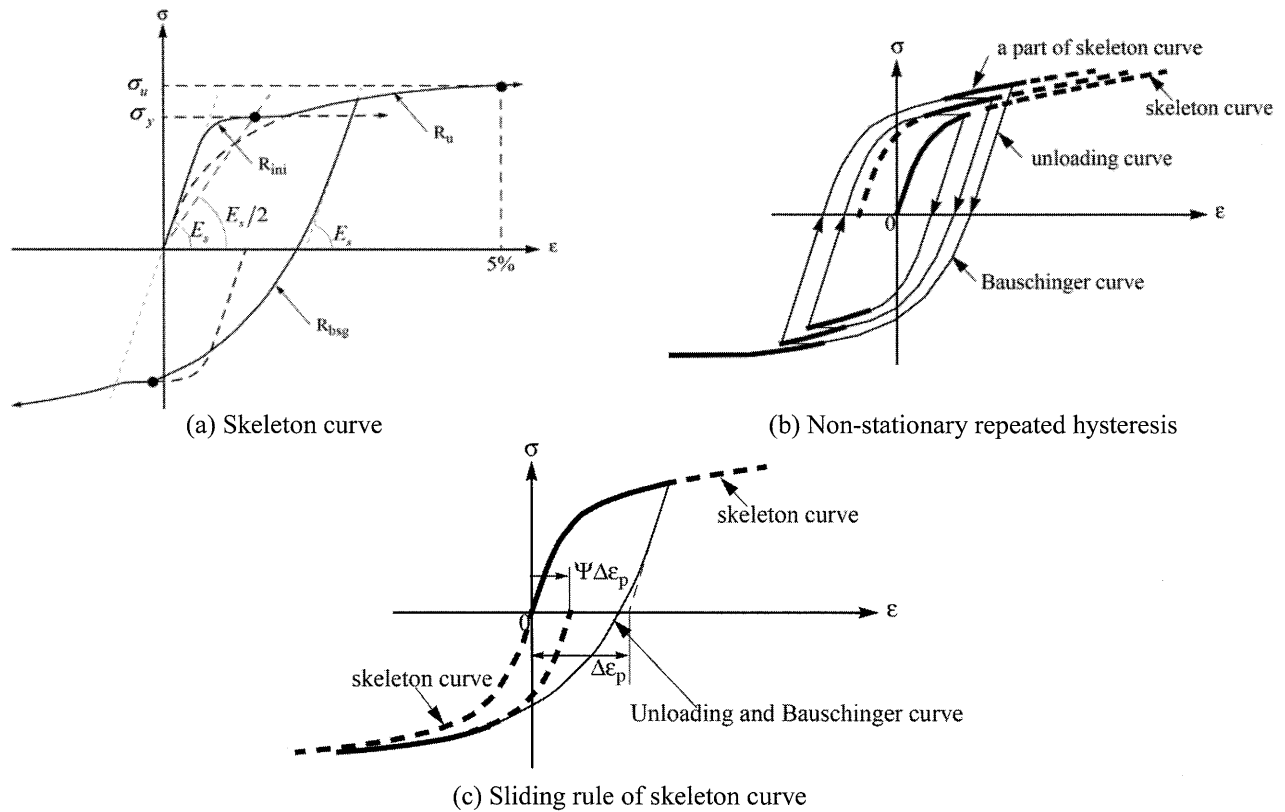


Fig. 4 Stress-strain relationship of steel fiber

Table 1 Parameter used in the steel fiber and concrete fiber model

| | Parameters | Square CFT and Diamond CFT | Circular CFT |
|--|----------------------------|----------------------------|---------------------|
| Concrete | Young's modulus | E_c | |
| | Compressive strength f_c | $1.1_c \sigma_B$ | $1.1_c \sigma_{cB}$ |
| Steel | Young's modulus | E_s | |
| | Yield stress σ_y | $1.1_s \sigma_y$ | |
| | Ultimate stress σ_u | $1.1_s \sigma_u$ | |
| ${}_c \sigma_{cB} = {}_c \sigma_B + \frac{1.56 {}_s t \cdot {}_s \sigma_y}{{}_s D - 2 {}_s t}$ | | | |

the circumference direction. The concrete core is subdivided into three segments in the radius direction and two segments in the circumference direction.

The square CFT member is divided into horizontal segments as shown in Fig. 2 (b). Two layers in the upper and lower steel tube are enough to account for flexural deformation of the steel tubes. With respect to the diamond shaped cross section CFT member, the concentrated section represented by solid circle are used. It is subdivided into twenty-one longitudinal fibers consisted of 21 concentrated sections of steel portion and 19 concentrated sections of concrete portion, as shown in Fig.2 (c). An appropriate stress and strain relationship must be assigned to each fiber element.

2.2.2 Models of Stress-Strain Relationships for Concrete and Steel

The stress-strain relationship model for a concrete fiber

in Fig. 3 consists of Popovics model⁷⁾ for the ascending part, and Sakino's model⁸⁾ for after yielding, where the tensile strength is omitted. The unloading and reloading paths are the straight lines as shown in Fig.3. In the analysis here, it is assumed that the strength in compression is kept constant as the compressive strain increases, which means the coefficient $\tau = 0$, in order to take the account of the confining effect of concrete encased in steel tube.

With respect to steel, the monotonic stress-strain relationship (skeleton curve) is expressed by a combination of two curves, each of which is the M&P function⁹⁾ as shown in Fig. 4 (a). The R_{ini} (=5.0) and R_u (=0.9) indicated in Fig. 4 (a) are the parameters to specify the roundness of curves, which values are adjusted to match the average curve of cold-formed mild steel tubes.

The non-stationary repeated hysteresis of steel is based

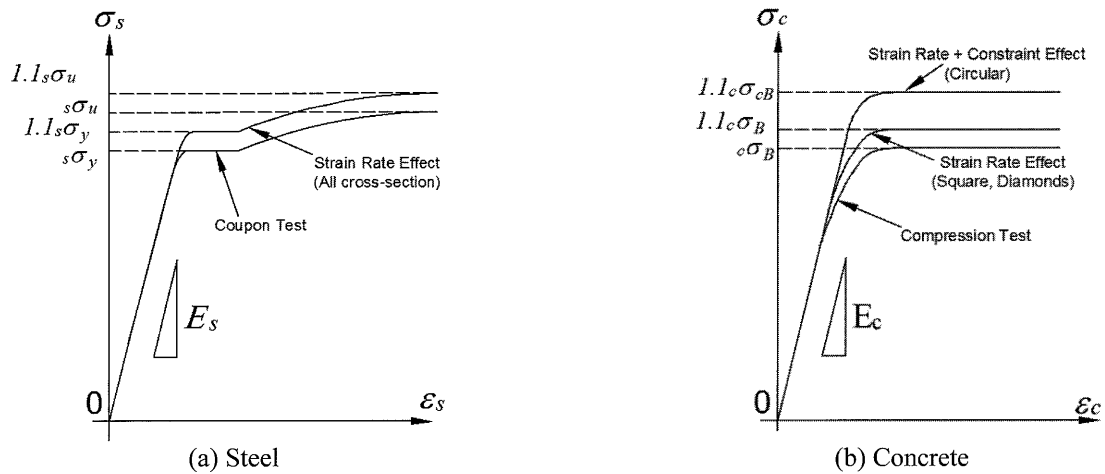


Fig. 5 Stress-strain relationship models for steel and concrete considering strain rate effect

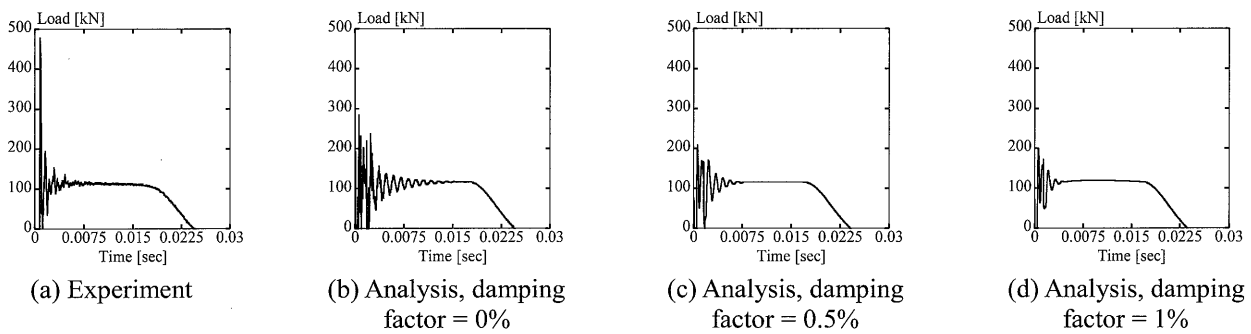


Fig. 6 Effect of damping factor on response of CFT member under impact load (Specimen Cfi3)

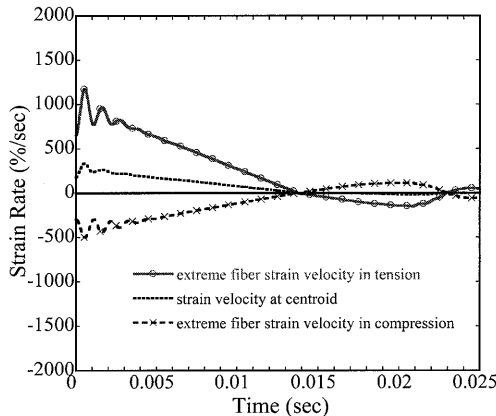


Fig. 7 Time histories of strain rates by analysis (Specimen Cfi3)

on the Ohi model¹⁰), in which a cyclic hysteresis curves consist of a part of the skeleton curve, and the unloading and Bauschinger curve as shown in Fig. 4 (b). A part of the skeleton curve slides horizontally and is used as a part of the hysteresis curve as shown in Fig. 4 (c). The amount of sliding is given by $\Psi \Delta \varepsilon_p$, where $\Delta \varepsilon_p$ is the increment of plastic strain in the previous opposite loading, and Ψ is the empirical coefficient with a typical value of 0.8. The unloading and Bauschinger curve is also expressed by the M&P function, where the parameter for roundness of the curve is taken as 1.2.

It is well known that the material strengths of steel and

concrete increase under the high strain rate. The compressive strength of concrete f_c for impact response analysis is magnified as 1.1 times of that obtained by the material testing (${}_c\sigma_B$). Simultaneously, both of the yield stress σ_y and the ultimate stress σ_u are magnified as 1.1 times of those by the material testing (${}_s\sigma_y$ and ${}_s\sigma_u$, respectively). The factor of 1.1 is determined in consideration of the experimental results²). With respect to compressive strength of circular CFT members ${}_c\sigma_{cB}$, the compressive strength of concrete by material testing (${}_c\sigma_B$) is further magnified by the confining effect according to AIJ Recommendations¹¹). The material properties used for steel and concrete models in the impact response analysis are shown in Table 1. Fig. 5(a) and (b) indicate the stress-strain relationships of steel tube and infill concrete considering strain rate effect.

2.2.3 Damping Factor

The damping factor for the analysis model is verified with the experiment results²). The damping is given by the Rayleigh damping with same damping factors. The experimental result (circular CFT specimen Cfi3 with the mass of striker = 267kg and the dropping height = 2500mm) is compared with analysis for cases that the damping

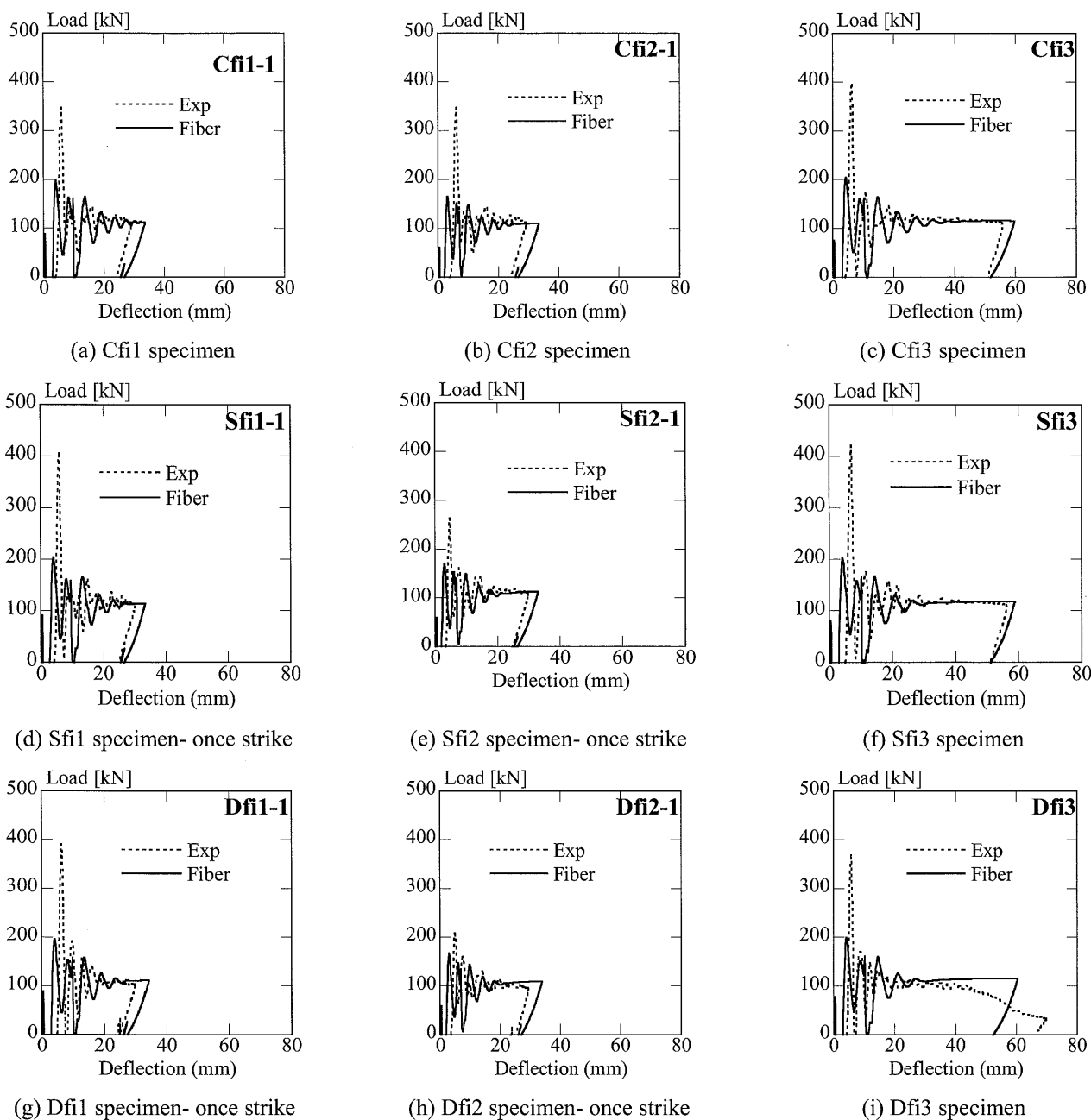


Fig. 8 Lateral impact load-deflection relationship comparison of CFT specimens between experiment results and fiber element analysis

factors of the primary and the third modes are 0%, 0.5% and 1% as shown in Fig. 6. From the comparison, the structural response for 0.5% damping is the same as that of the experiment so the damping factor is set as 0.5%.

2.2.4 Effect of Strain Rate

The high strain rate (velocity) increases the yield strength and the ultimate strength of steel tubes, and the compressive strength of concrete. From the formulae specified by the Japan Society of Civil Engineers^[2], each strength may increase up to around 120%, if the strain rate exceeds 100%/sec.

Fig. 7 shows the time histories of strain rates of a circular

CFT specimen (Cfi3) simulated by the analysis. From the figure, the strain rates at extreme fiber in tension and at that in compression exceeds beyond 100%/sec until progress 0.014sec, that is the collision duration with the striker.

The dynamic magnification factor of 1.1, which has been adopted in the clause 2.2.2, is smaller than that by the strain rate effect. On the other hand, the damping factor also increases the resistance of a member, and the factor of 0.5% has been adopted in the clause 2.2.3. The 120% strength increase of a member in the impact response analysis is realized by the combination of the dynamic magnification factor and the damping factor.

Table 2 Summary of comparison between experiment and analysis

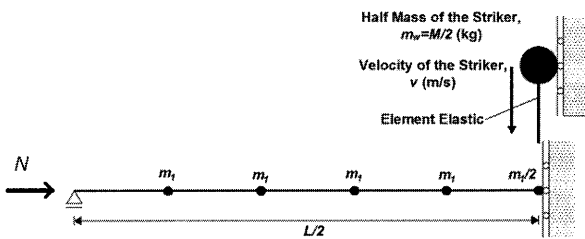
| Name of specimen ²⁾ | Striker | | Maximum deflection δ_m | | | Residual deflection δ_r | | | Energy absorption | | |
|--------------------------------|-------------|-------------|-------------------------------|------------------|------------------|--------------------------------|------------------|------------------|-------------------|-----------------|------------------|
| | h (mm) | M (kg) | Test (mm) | Analysis (mm) | Analysis Test | Test (mm) | Analysis (mm) | Analysis Test | Test (J) | Analysis (J) | Analysis Test |
| Cfi1-1 | 2500 | 142 | 29.3 | 33.7 | 1.15 | 23.9 | 25.4 | 1.06 | 2894 | 2998 | 1.04 |
| Cfi2-1 | 1250 | 267 | 29.2 | 33.4 | 1.15 | 23.3 | 25.5 | 1.09 | 2801 | 2895 | 1.03 |
| Cfi3 | 2500 | | 55.7 | 59.7 | 1.07 | 49.2 | 50.6 | 1.03 | 5939 | 5945 | 1.00 |
| Sfi1-1 | 2500 | 142 | 29.9 | 33.4 | 1.12 | 24.2 | 25.3 | 1.05 | 2916 | 3006 | 1.03 |
| Sfi2-1 | 1250 | 267 | 29.7 | 33.0 | 1.11 | 24.1 | 25.3 | 1.05 | 2839 | 2903 | 1.02 |
| Sfi3 | 2500 | | 56.3 | 58.7 | 1.04 | 50.1 | 50.0 | 1.00 | 6011 | 5952 | 0.99 |
| Dfi1-1 | 2500 | 142 | 29.9 | 34.3 | 1.15 | 24.5 | 25.9 | 1.06 | 2687 | 3011 | 1.12 |
| Dfi2-1 | 1250 | 267 | 29.3 | 33.9 | 1.16 | 23.7 | 26.0 | 1.10 | 2536 | 2905 | 1.15 |
| Dfi3 | 2500 | | 69.8 | 60.4 | 0.87 | 65.6 | 51.1 | 0.78 | 5891 | 5942 | 1.01 |

Table 3 Analysis model subjected to constant axial load

| Name of specimen ²⁾ | Cross section | $sD (sB) \times_s t \times L$ (mm) | Ultimate axial force, N_u (kN) | Mass and dropping height of striker | |
|--------------------------------|---------------|---------------------------------------|-------------------------------------|-------------------------------------|----------|
| | | | | M (kg) | h (mm) |
| Cfi3 | Circular CFT | 114.3×3.5×1000 | 1222 | $M_b+17\text{kg}$ | 2500 |
| Sfi3 | Square CFT | 100×3.2×1000 | 1073 | | |
| Dfi3 | Diamond CFT | 100×3.2×1000 | 1073 | | |

Note : N_u is ultimate axial force of a CFT member based on the Recommendations by AIJ (2008)¹¹⁾.

$M_b = \alpha \times M_o$, M_o = back up steel mass = 250kg and α = magnification factor

**Fig. 9** Analysis model subjected to constant axial load

3. Analytical Results

3.1 Comparison between Load-Deflection Relationships by Experiment and Analysis

Fig. 8 shows the comparison between the load-deflection relationship by experiment (dashed line) and that by analysis (solid line). The circular CFT specimens are indicated in Figs. 8(a), (b) and (c), the square CFT specimens in Figs. 8(d), (e) and (f) and the diamond shaped CFT specimen in Figs. 8 (g), (h) and (i), respectively.

Impact response capacity is related more closely to energy absorption than to a maximum measured load¹³⁾. According to El-Tawil et al.¹⁴⁾, the peak load generated at the impact is not representative of the design structural demand, as the structures do not have enough time to respond to a rapid change of loading. Therefore, the comparison should be done for the lateral impact load-deflection relationship after the initial impact load.

The good agreement has been found in the results between experiment and fiber element analysis. With respect to the diamond shaped CFT specimen Dfi3 (Fig. 8 (i)), though the specimen deteriorates by crack of a tube in the experiment, the analysis cannot reproduce the phenomenon because the

stress-strain relationship model ignores the crack.

The summary is shown in Table 2. The ratio of the maximum deflection δ_m ranges from 1.04 to 1.16 and the residual deflection δ_r from 1.00 to 1.10 except for the specimen Dfi3, which fails by local buckling with the steel tube crack. The energy absorption is directly calculated by integrating the area under the lateral impact load-deflection relationship. The ratio of the energy absorption by the analysis to that by the experiment ranges from 0.99 to 1.04 except for the Dfi1-1 which fails by local buckling of the steel tube and Dfi2-1 which fails by local buckling with the steel tube crack²⁾. From the energy absorption comparison, it may be said that the analysis model successfully reproduce the experimental results.

3.2 Stable Limit of CFT member to Sustain Axial Load under Transverse Impact Loading

3.2.1 Analytical Model Subjected to Constant Axial Load

The analysis model for a CFT member subjected to constant axial load is similar to the model of the member without axial load as shown in Fig. 9. The constant axial load applies at the end of the specimen during the impact loading.

The increases due to the strain rate effect are also taken into account in the yield stress, the ultimate stress of steel a tube and the maximum compressive stress of concrete as shown in Table 1. The specimens for the analysis model subject to constant axial load can be seen in Table 3.

3.2.2 Conversion and Diversion of Deflections

The axial load level are represented by the axial load ratio n which is defined as the ratio of the applied load N to the ultimate axial load predicted by AIJ¹¹⁾ N_u . Figs. 10 (a) to (e)

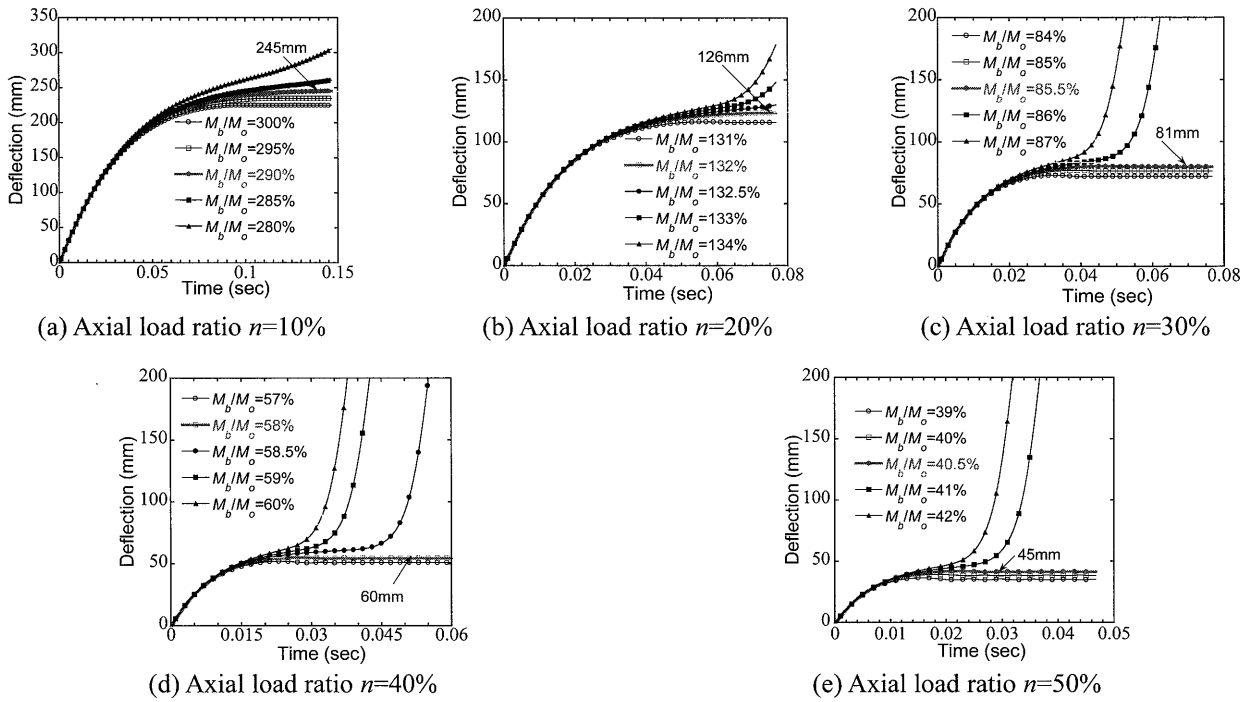


Fig. 10 Lateral deflection-time relationship by impact response analysis of circular CFT specimens

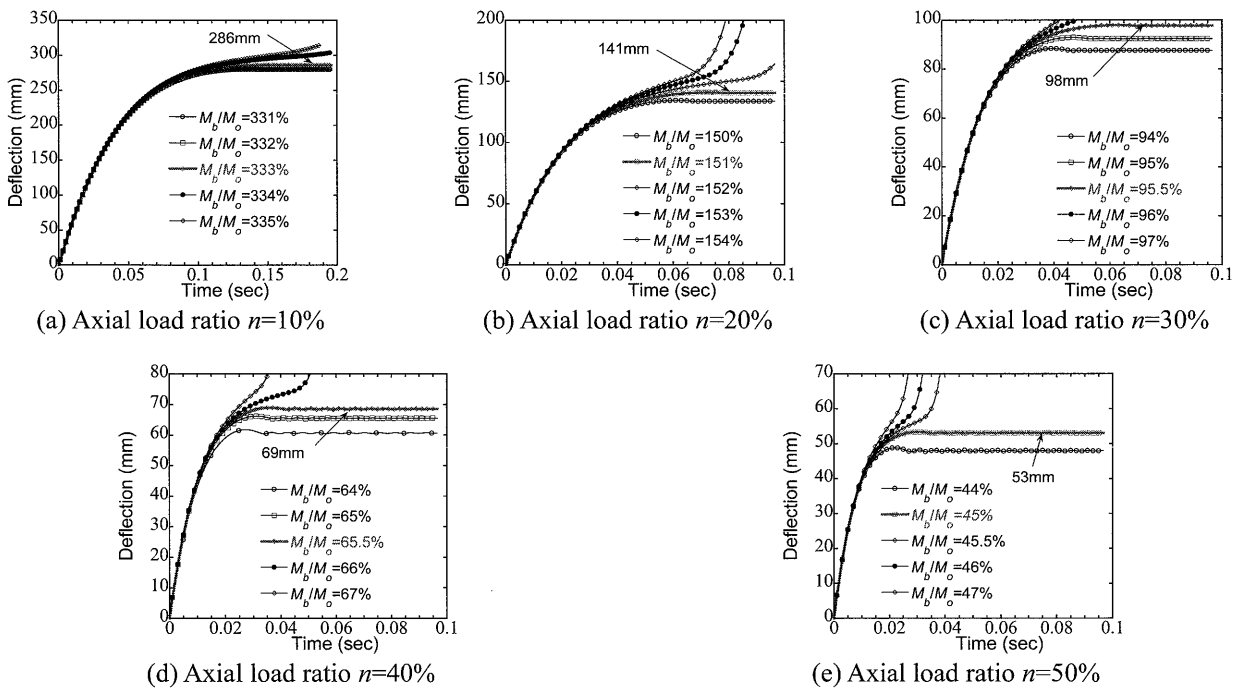


Fig. 11 Lateral deflection-time relationship by impact response analysis of square CFT specimens

show lateral deflection-time relationship of circular CFT specimens under constant axial load ratio n of 10%, 20%, 30%, 40% and 50%, respectively. The magnification factor for striker mass is studied to include the boundary between conversion and diversion of deflection. The solid line represents the ultimate state for conversion. The ultimate mass of the striker for the conversion becomes larger as the axial load ratio becomes smaller. Simultaneously, the ultimate deflection for the conversion u_{cr} becomes larger as the axial load ratio becomes smaller.

Fig. 11 and Fig. 12 show the deflection-time relationships of square CFT specimens and those of diamond shaped CFT specimens, respectively. The similar phenomena appear in these cases.

Thus, it becomes clear that there is the ultimate mass of the impact load for the deflection not to diverge at a certain axis load ratio. It can be expressed the mass of the impact strength in other words with the magnitude of input energy by the impact load, because the dropping height of the striker is kept constant as 2500mm.

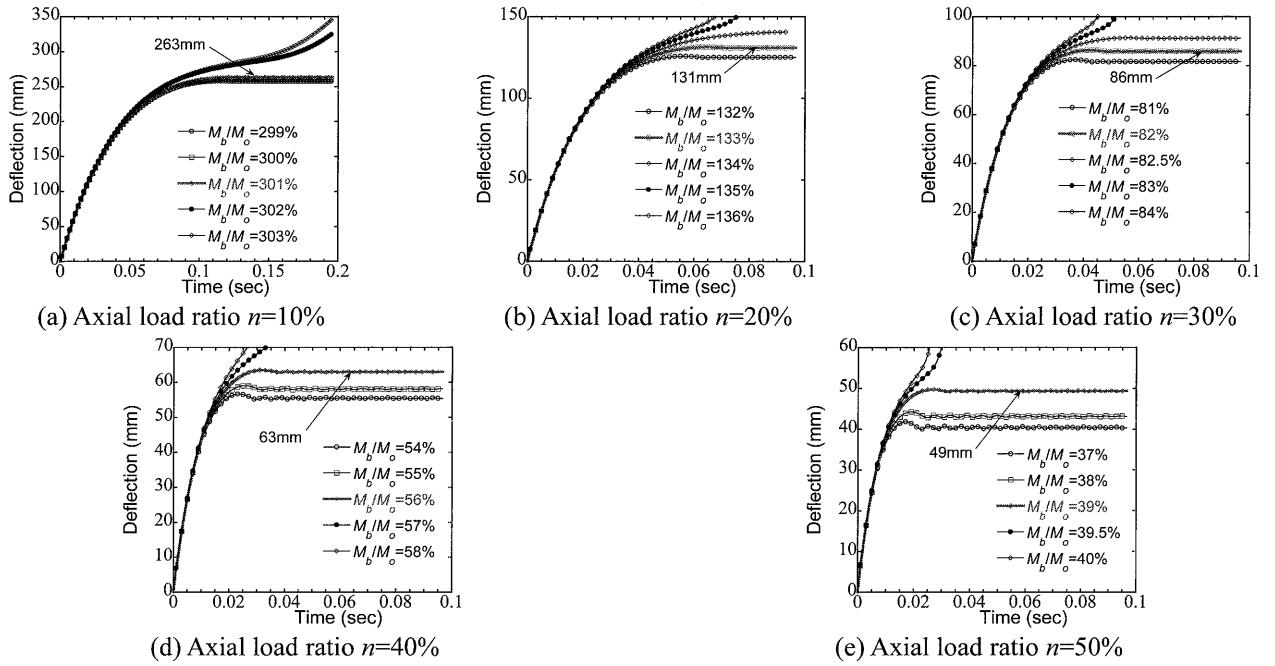


Fig. 12 Lateral deflection-time relationship by impact response analysis of diamond CFT specimens

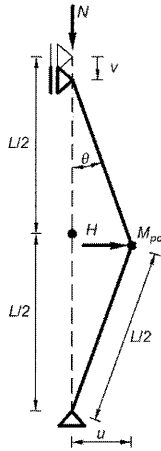


Fig. 13 Plastic collapse mechanism of CFT member

4. Evaluation Method for Impact Capacity of CFT Member

4.1 Energy Balance for CFT Member Model of Plastic Analysis

Fig. 13 indicates the plastic collapse mechanism of the model of a CFT member for the plastic analysis. The model is subjected to the constant compressive axial load N and the impact transverse load H at the mid span. The plastic hinge forms at the mid-span of the member as shown by the solid circle, where the hinge moment is the full plastic moment taking the account of the axial force M_{pc} .

Let us consider about the energy for the plastic collapse mechanism. The work done by the axial load E_N is represented by the following equation.

$$E_N = Nv \quad (1)$$

Similarly, the total work by impact load E_H is

represented by Eq. (2), where the integration range is the collision duration Δt .

$$E_H = \int_{t=0}^{\Delta t} H(t)u(t)dt \quad (2)$$

The energy absorbed at the plastic hinge E_{pl} is given by Eq. (3), where the term of $N\Delta L_p$ (ΔL_p : compressive axial strain at the center of gravity in the cross section) is not influential and then it is omitted by the discussion afterward.

$$E_{pl} = M_{pc}(2\theta) + N\Delta L_p \cong M_{pc}(2\theta) \quad (3)$$

The following equations are obtained from the geometric relationships of the plastic collapse mechanism of a CFT member shown in Fig. 13.

$$u = \frac{L}{2} \sin \theta \quad (4)$$

$$v = L \cdot (1 - \cos \theta) \quad (5)$$

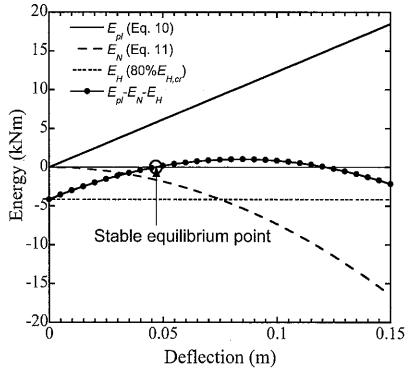
The following approximations are introduced.

$$\sin \theta = \frac{2u}{L} \cong \theta \quad (6)$$

$$\cos \theta = \sqrt{1 - (\sin \theta)^2} = \sqrt{1 - \left(\frac{2u}{L}\right)^2} \cong 1 - \frac{1}{2} \left(\frac{2u}{L}\right)^2 \quad (7)$$

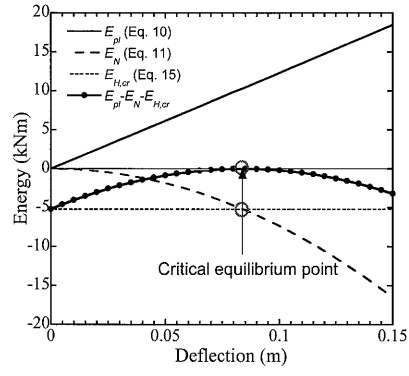
Substituting Eq. (7) to Eq. (5), the following expression is obtained.

$$v = \frac{L}{2} \left(\frac{2u}{L}\right)^2 \quad (8)$$



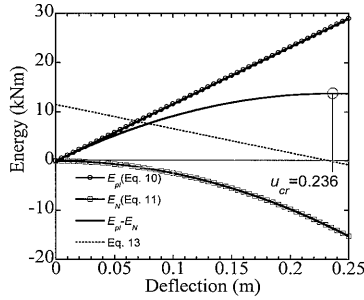
(a) Stable equilibrium ($n=30\%$)

($E_H=80\%$ of ultimate energy of impact load $E_{H,cr}$)

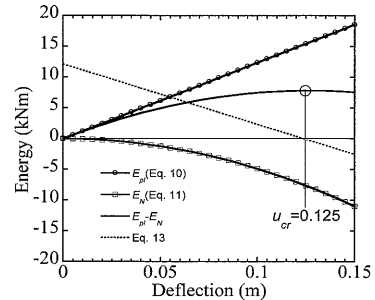


(b) Critical equilibrium ($n=30\%$)

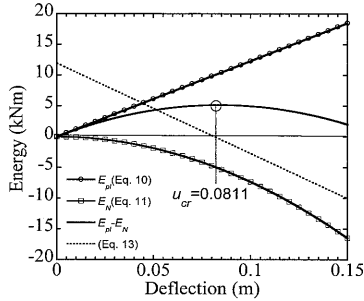
Fig. 14 Equilibrium state of circular CFT specimens, $n=30\%$



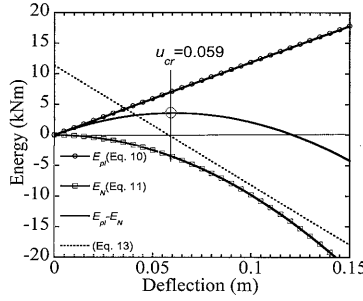
(a) $E_{pl}-E_N$ of $n=10\%$



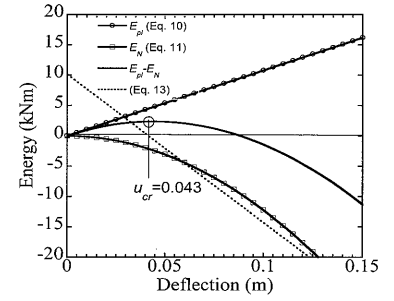
(b) $E_{pl}-E_N$ of $n=20\%$



(c) $E_{pl}-E_N$ of $n=30\%$



(d) $E_{pl}-E_N$ of $n=40\%$



(e) $E_{pl}-E_N$ of $n=50\%$

Fig. 15 Equilibrium of circular CFT

From the principle of virtual work, the following equation is established.

$$\Pi = E_{pl} - E_N - E_H = 0 \quad (9)$$

From Eqs. (3), (4) and (6), the following equations are derived.

$$E_{pl} = M_{pc} \left(\frac{4u}{L} \right) = \frac{4M_{pc}u}{L} \quad (10)$$

Similarly, from Eqs. (1) and (5), the following equations are obtained.

$$E_N = N \cdot \frac{L}{2} \left(\frac{2u}{L} \right)^2 = N \cdot \frac{2u^2}{L} \quad (11)$$

By substituting Eqs. (10) and (11) into Eq. (9), the following equation is established.

$$\Pi = \frac{4M_{pc}u}{L} - N \cdot \frac{2u^2}{L} - E_H = 0 \quad (12)$$

The structural system is in the equilibrium state, when the Π is equal to zero.

Fig. 14 (a) indicates the relationship of the energy function Π (solid line with solid circles) and the deflection, where the components of the E_{pl} , the E_N and the E_H are also indicated. The E_H for Fig. 14(a) is 80% of $E_{H,cr}$ ($=5\text{kNm}$). The equilibrium point is plotted by the circle, where the function Π is zero. Let us consider the case that the deflection increases virtually. As shown in the figure, when the deflection increases, the function Π increases. This means the energy absorption by the plastic hinge E_{pl} is prior to the work done by the axial load E_N , and then the equilibrium state can be said to be stable.

On the other hand, the equilibrium point indicated in Fig.

Table 4 Comparison between u_{cr} by plastic analysis and that by impact response analysis

| $n = \frac{N}{N_u}$ | | Circular CFT (Cf3) | | Square CFT (Sf3) | | Diamond CFT (Df3) | |
|---------------------|--------------------------|--------------------|-------------------------------|------------------|-------------------------------|-------------------|-------------------------------|
| | | u_{cr} [m] | $\frac{u_{cr,PL}}{u_{cr,IM}}$ | u_{cr} [m] | $\frac{u_{cr,PL}}{u_{cr,IM}}$ | u_{cr} [m] | $\frac{u_{cr,PL}}{u_{cr,IM}}$ |
| 0.1 | Plastic Analysis | 0.236 | 0.96 | 0.296 | 1.04 | 0.280 | 1.06 |
| | Impact Response Analysis | 0.245 | | 0.286 | | 0.263 | |
| 0.2 | Plastic Analysis | 0.125 | 1.01 | 0.150 | 1.06 | 0.142 | 1.08 |
| | Impact Response Analysis | 0.124 | | 0.141 | | 0.131 | |
| 0.3 | Plastic Analysis | 0.081 | 1.00 | 0.100 | 1.02 | 0.093 | 1.08 |
| | Impact Response Analysis | 0.081 | | 0.098 | | 0.086 | |
| 0.4 | Plastic Analysis | 0.059 | 0.98 | 0.073 | 1.05 | 0.069 | 1.09 |
| | Impact Response Analysis | 0.060 | | 0.069 | | 0.063 | |
| 0.5 | Plastic Analysis | 0.043 | 1.02 | 0.056 | 1.05 | 0.052 | 1.06 |
| | Impact Response Analysis | 0.042 | | 0.053 | | 0.049 | |

Note: $u_{cr,PL}$ is the u_{cr} by plastic analysis, $u_{cr,IM}$ is the u_{cr} by impact response analysis.

14 (b) is just on the peak of the energy function Π . In this case, if the deflection increases from the point even a little, then the function Π decreases which means that the system becomes unstable. Therefore, the equilibrium state as shown in Fig. 14 (b) can be said the critical equilibrium state.

The energy E_H just on the critical equilibrium state is here called as the ultimate energy of impact load $E_{H,cr}$.

4.2 Critical Deflection

The energy function Π is the function of deflection u . As shown in Fig. 14 (b), the Π must satisfy the following equation at the critical equilibrium point, so that the Π is the maximum at the point.

$$\frac{d\Pi}{du} = \frac{4M_{pc}}{L} - N \cdot \left(\frac{4u}{L} \right) = 0 \quad (13)$$

From Eq. (13), the following equation is obtained.

$$u_{cr} = \frac{M_{pc}}{N} \quad (14)$$

The u_{cr} is the deflection at the critical equilibrium state. In other words, if the deflection u exceeds the critical deflection u_{cr} , then the member cannot support the axial load anymore.

Figs. 15 (a) to (e) show the energy $E_{pl} + E_N$, the equilibrium states and the critical deflections u_{cr} of the circular CFT specimens for various axial load ratios. It is seen that the u_{cr} decreases as the axial load ratio n increases. The numeric values for u_{cr} in the figure are obtained from Eq. (14). The thin dotted lines indicate Eq. (13), which intersect the horizontal axes at the critical equilibrium points. Similar phenomena have been confirmed for the square CFT specimens and the diamond shaped CFT specimens as well, even the results are not shown here.

4.3 Verification of Critical Deflection by Impact Response Analysis

Table 4 shows the comparison between u_{cr} by Eq. (14) of the plastic analysis and that by the impact response analysis which is obtained from the clause 3.2. It is seen in the figure that the critical deflection u_{cr} by the plastic analysis is almost same as that by the impact response analysis. Therefore, It can be said that Eq. (14) derived from the plastic analysis is available to predict the ultimate input energy of the striker.

5. Ultimate Lateral Impact Energy Calculation of CFT Specimens

Here, Eqs. (9), (10), (11) and (14) are listed up again.

$$\Pi = E_{pl} - E_N - E_H = 0 \quad (9)$$

$$E_{pl} = M_{pc} \left(\frac{4u}{L} \right) = \frac{4M_{pc}u}{L} \quad (10)$$

$$E_N = N \cdot \frac{L}{2} \left(\frac{2u}{L} \right)^2 = N \cdot \frac{2u^2}{L} \quad (11)$$

$$u_{cr} = \frac{M_{pc}}{N} \quad (14)$$

Eq. (14) indicates the critical equilibrium state. From the above equations, the following equation is derived.

When $u = u_{cr}$

$$\begin{aligned} E_{H,cr} = E_{pl,cr} - E_{N,cr} &= \frac{4M_{pc} \cdot u_{cr}}{L} - \frac{2N \cdot u_{cr}^2}{L} \\ &= \frac{4M_{pc} \cdot u_{cr}}{L} - \frac{2M_{pc} \cdot u_{cr}}{L} = \frac{2M_{pc} \cdot u_{cr}}{L} \end{aligned} \quad (15)$$

Where $E_{H,cr}$, $E_{pl,cr}$ and $E_{N,cr}$ are the E_H , E_{pl} and E_N when the u is equal to the u_{cr} .

On the other hand, u may be specified as u_{limit} in a structural design such as reasons of the crack of steel tube or the serviceable or the repairable requirement. In this case, the

u must be less than the u_{cr} . From Eq. (9), (10) and (11), the following equation is derived.

When $u < u_{cr}$

$$E_{H,lim} = E_{pl,lim} - E_{N,lim} = \frac{4M_{pc} \cdot u_{lim}}{L} - \frac{2N \cdot u_{lim}^2}{L} \quad (16)$$

Where $E_{H,lim}$, $E_{pl,lim}$ and $E_{N,lim}$ are the E_H , E_{pl} and E_N when the u is equal to the u_{limit} .

The boundary condition of a CFT member in a real structure may be different from the pin-pin supports such as the model. In this case, energy absorptions by plastic hinges at the top and the bottom of the member may be taken into account for energy absorption E_{pl} .

6. Conclusive Remarks

Some comments regarding this study are worth noting:

1. The frame analysis model accurately predicts the experimental impact responses except for specimens with cracks of tubes.
2. From a parametric numerical study by using the analytical model, it is clarified that the deflection of CFT member under the constant compressive axial load diverges when the axial load ratio is high. There exists the critical equilibrium state where the deflection is the upper limit so as not to diverge, which is called here as the critical deflection. Corresponding to the critical equilibrium state, there exists the ultimate intensity or the energy of input energy by the impact load for each axial load ratio.
3. By the plastic analysis using a plastic-hinge model, the evaluation equations are derived for the critical deflection and the ultimate energy of impact load of a CFT member under impact loading. The precision of the formula for the critical deflection is confirmed by the comparison with the impact analysis.
4. A design formulae are proposed for the allowable input energy of impact load for a CFT member under the constant axial load at the critical equilibrium state and at the a certain deflection is specified from the requirement of such as the repairable limit state.

Acknowledgement

This study is financially supported by the Scientific Research Grant (B) H25- H27 No. 25289186, Steel structure research and educational grant project H25, Ministry of Education, Culture, Sports, Science and Technology, Japan. One of the authors thanks the Indonesian Directorate of Higher Education Program (DIKTI) for a doctoral scholarship.

References

- [1] Kawano, A. and Warner, R. F.: Nonlinear analysis of the time-dependent behavior of reinforced concrete frames, Research Report No. R125, Department of Civil and Environmental Engineering, the University of Adelaide, 1995.
- [2] Effendi, M. K., Kawaguchi, H., Kawano, A., Ninakawa, T., Matsuo, S., Tsuda, K. and Kido, M. : Experimental investigation on dynamic responses of concrete-filled steel tubular members subjected to transverse impact loads, Journal of Architecture and Urban Design, Kyushu University, No. 24, pp. 97-106, 2014.
- [3] Yousuf, M., et al. : Impact behaviour of pre-compressed hollow and concrete-filled mild and stainless steel columns, Journal of Constructional Steel Research 96, pp. 54-68, 2014.
- [4] Wang, R., et al. : Behavior of concrete-filled steel tubular (CFST) members under lateral impact: Experiment and FEA model, Journal of Constructional Steel Research 80, pp. 188-201, 2013.
- [5] Han, L., et al. : Behaviour of high-strength concrete-filled steel tubes under lateral impact loading, Journal of Constructional Steel Research 92, pp. 25-39, 2014.
- [6] Fujikake, K., Li, B. and Soeun, S. : Impact response of reinforced concrete beam and its analytical evaluation, J. Struct. Eng., 135(8), pp.938–950, 2009.
- [7] Popovics, S. : A numerical approach to complete stress-strain curve of concrete, Cement and Concrete Research 3, pp.583-599, 1973.
- [8] Sakino, K. and Sun, Y. P. : Stress-strain curve of concrete confined by rectilinear hoop, Journal of Structural and Construction Engineering, AIJ, No. 461, pp. 95-104, 1994. [in Japanese]
- [9] Menegotto, M. and Pinto, P. E. : Method of analysis for cyclically loaded R. C. frames including changes in geometry and non-elastic behaviour of elements under combined normal force and bending, IABSE Congress Reports of the Working Commission, Band 13, 1973.
- [10] Meng, L., Ohi, K. and Takanashi, K. : A simplified model of steel structural members with strength deterioration used for earthquake response analysis, Journal of Structural and Construction Engineering, Architectural Institute of Japan, No. 437, 115-124, 1992.
- [11] Architectural Institute of Japan (AIJ): Recommendations for design and construction of concrete-filled steel tubular structures, October, 2008. (in Japanese)
- [12] Japan Society of Civil Engineers (JSCE): Impact behavior and design of structures, Structural Engineering Series 6, JSCE, Tokyo, 1993. [in Japanese]
- [13] Yousuf, M., et al.: Behavior and resistance of hollow and concrete filled mild steel columns due to transvers impact loading. Australian journal of structural engineering, 13, 65-80, 2012.
- [14] El-Tawil, S., et al.: Vehicle collision with bridge piers." J. Bridge Eng., 10(3), 345–353, 2005.

Appendix A. Impact Analysis by Earthquake Response Procedure

The seismic response analysis is applied to solve the

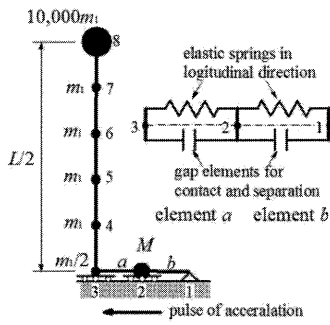


Fig. A.1 Fiber element segmentation of CFT specimens

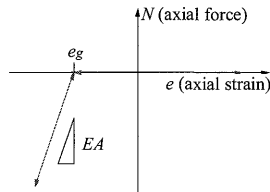


Fig. A.2 Gap element

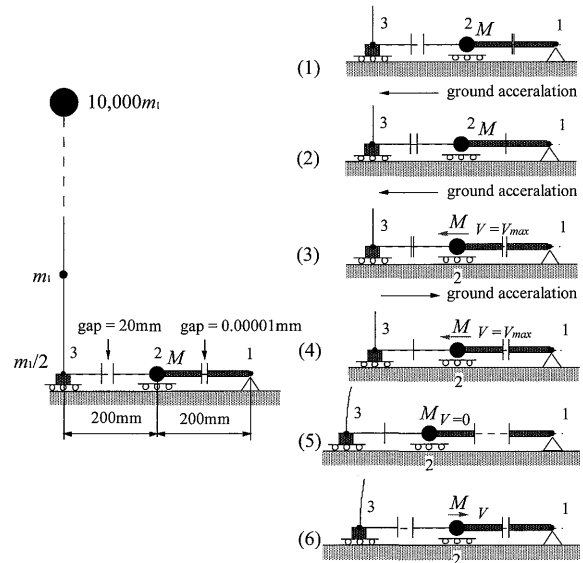
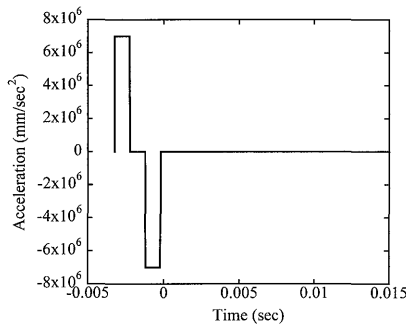
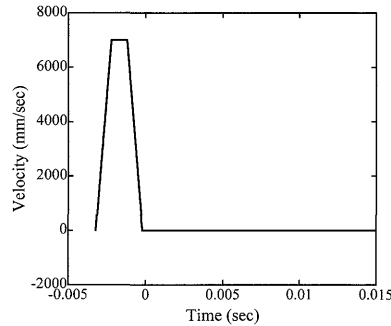


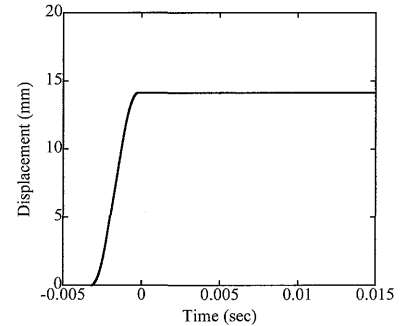
Fig. A.3 Process of collision between striker and specimen



(a) Ground acceleration



(b) Ground velocity



(c) Absolute ground displacement

Fig. A.4 Ground motion corresponding to Tsunami impact velocity

impact analysis. Fig. A.1 shows the analysis model. Node 1 is supported by a pin support on the ground. Node 2 contains mass of the dropping weight (striker) and is supported by roller support on the ground. Node 3 represents a node of the symmetrical center of a CFT member which is supported by roller support on the ground. The rotations are restraint in node 2 and node 3. Nodes 4 to 7 are nodes for element division. The node 8 has 10,000 times the mass of the lumped masses of nodes 4 to 7. Node 8 works as the pin roller support at the end of a simple beam. Lumped mass of the node 3 is set to half of the node 4 to 7 because of the symmetrical condition. Lumped masses are set to perpendicular and parallel directions to the ground surface except for the node 8, which is set only to the parallel direction to the ground surface.

The phenomenon of contact and separation is required in the impact analysis, which is realized by a gap element as shown in Fig. A.2 in this analysis. When the strain of the gap element exceeds the e_g , then the element loses stiffness and strength. On the other hand, the strain is equal to or less than the e_g , then the element becomes an elastic body. The elastic stiffness of gap element can be set large enough for the collision.

The elements a and b are composed of the gap elements and elastic springs as shown in Fig.A.1. Each of elastic springs has very small stiffness just to make the system stable. The gap element has the equivalent stiffness as the steel cylinder with 200 mm in diameter of the striker. The initial gap e_g in element a is set -20mm, within which the mass M as the striker subjected to impulse acceleration reaches the specified velocity.

Process of Collision

As shown in Fig. A.3, the process of the collision between the striker and the specimen is as follows:

1. Node 1 is applied by impulse ground acceleration resulting the velocity of Tsunami flotsam as shown in Fig. A.4. Node 2 moves together with Node 1. [processes of (1) and (2)]
2. When Node 2 moves 20 mm which is the initial gap e_g of element a , the mass M of node 2 collides to Node 3 which is the mid-span of the CFT member. [processes of (3) and (4)]
3. The deflection of CFT member increases and reaches the maximum, at which the velocity of Node 3 is zero. [processes of (5)]

4. CFT member rebound in elastic, the mass M is moved in the opposite direction. [process of (6)]

Fig. A.4 shows the impulse ground acceleration, corresponding ground velocity and absolute ground displacement. The peak of the ground velocity is 7000mm/sec, which is corresponds to Tsunami flotsam velocity.

(受理：平成27年 6 月11日)